CHEMISTRY OF MATERIALS

ARTICLE

pubs.acs.org/cm

Monitoring the Formation of H-MCM-22 by a Combined XRPD and Computational Study of the Decomposition of the Structure Directing Agent

Luca Palin, Gianluca Croce, Davide Viterbo, and Marco Milanesio*

Dipartimento di Scienze e Tecnologie Avanzate and Nano-SiSTeMI Interdisciplinary Centre, Università del Piemonte Orientale "Amedeo Avogadro", Viale T. Michel 11, 15121 Alessandria, Italy

Supporting Information

ABSTRACT: MCM-22 is a siliceous microporous material with the MWW topology. The MCM-22 precursor is a partially disordered layered material that contains hexamethyleneimine (HMI) as the structural directing agent. The layered phase transforms into the ordered three-dimensional zeolite at 523 K, still retaining HMI molecules inside the cages and the channels. Four different samples were analyzed by high resolution synchrotron radiation powder diffraction, after thermal treatment at 373, 523, 623, and 823 K when the organic phase is completely removed. The localization of the HMI molecules was done by direct space Monte Carlo methods and using maximum entropy maps. The disordered molecules were localized in the 10-member ring (MR) sinusoidal channels, in the 12-MR inner part of the supercage and in the 10-MR crossing window. In the precursor, heated at 373 K, there is evidence that the different lamellar sheets are not completely connected one to the other. Molecular orbital (MO) theoretical calculations, applying both periodic and cluster approaches, were performed to shed light on the real symmetry of the calcined MCM-22 phase and on the features of the interlayer interactions in the MCM-22 precursor.

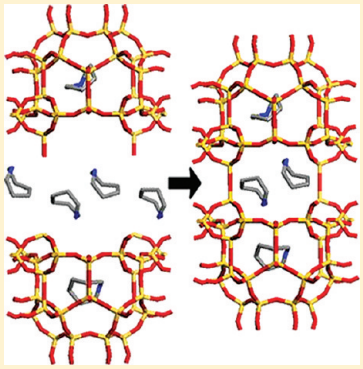

KEYWORDS: MCM-22 zeolite, synchrotron X-ray powder diffraction, theoretical calculations, structural transitions, template location

1. INTRODUCTION

MCM-22 zeolite (IZA code MWW) was discovered and characterized in 1990 by Mobil researchers,[1] even though a previous patent[2] refers to a material named PSH-3 that showed similar features. It is synthesized from silica and sodium silicate using hexamethyleneimine (HMI) (Figure 1) as the directing agent, in an aqueous, alkaline gel, in SiO_2/Al_2O_3 molar ratios from 30 to 100. Several applications are proposed in the literature.[3−5]

Generally, hydrothermal crystallization is conducted under stirring, but this material can be prepared in static conditions, as well. On passing from a material prepared under static to another prepared under dynamic conditions, the only observed change is the morphology of the crystals.[6]

The as-prepared material, known as *MCM-22 precursor*, is a layered solid that condenses into a tridimensional zeolitic structure upon heating (Figure 2). In the precursor sample, the layers themselves are approximately 12 Å thick and already display the 10-membered ring (MR) sinusoidal channels.[7,8] The surface is not smooth but shows external pockets, or cups, that will form supercavities when the layers condense.[8]

The layered precursor is structurally more disordered than a zeolitic structure, as evidenced by the wide, overlapping, poorly resolved peaks in its XRD profile (see Figures 3 and 4). The void spaces in the precursor structure have been shown by ^{13}C NMR,[9]

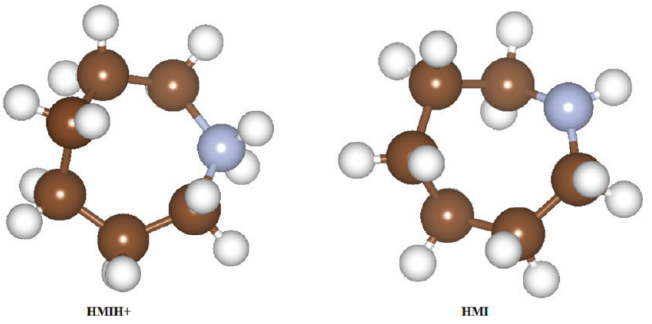

Figure 1. Molecular structures of $HMIH^+$ and HMI (brown, C; blue, N; and white, H).

infrared spectroscopy,[10] and chemical analysis[11] to be filled with water, neutral HMI, and protonated HMI, herein called $HMIH^+$. The content of sodium ions in the precursor is negligible or nil, with the larger part of aluminum being compensated by $HMIH^+$.[6,12] However, the total organic content, obtained from TGA data, is higher than the aluminum content in the crystals,[11]

Received: May 24, 2011
Revised: October 1, 2011
Published: October 19, 2011

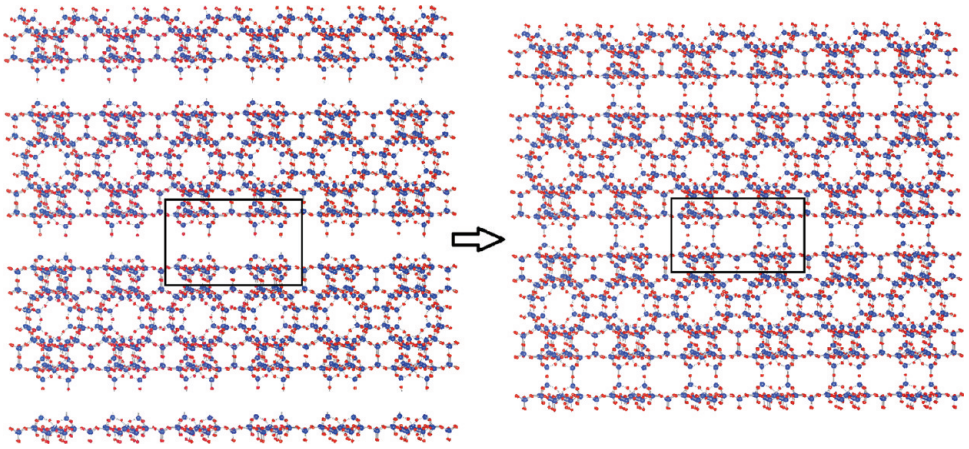

Figure 2. Condensation of the layered precursor (373 K sample on the left) into the 3D MCM-22 zeolite (823 K sample on the right). The black line rectangles highlight the cluster models used for the theoretical calculations and depicted in Figure 5; the layers are depicted unrealistically separated in order to highlight the investigated transformation.

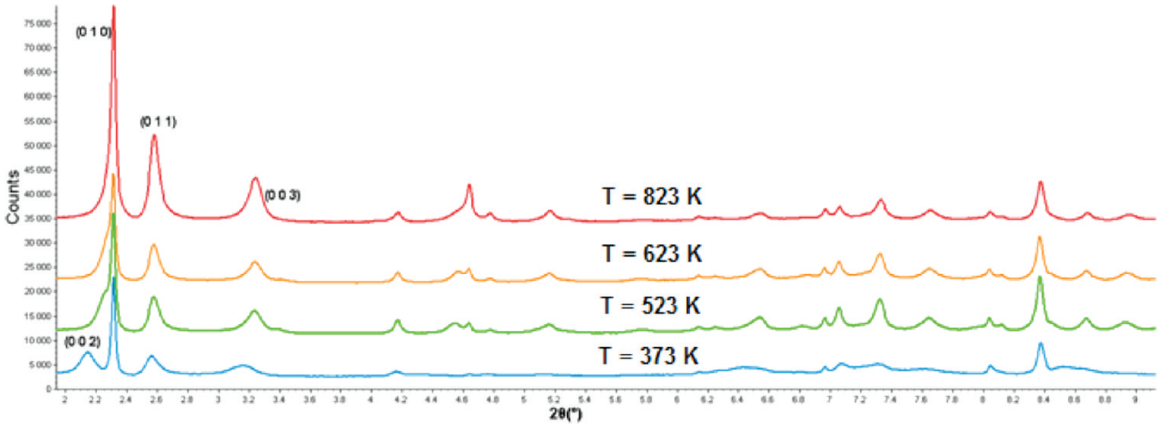

Figure 3. XRPD patterns of the four different samples during the template removal process.

indicating that neutral organic material might be occluded, together with water, in the interlayer or intralayer spaces. It is precisely the thermal elimination of the organic and water molecules from the interlayer space that allows the approaching of the layers and favors their condensation into the final structure. ^{13}C-MAS NMR of the precursor showed large peaks for the carbon nuclei immediately neighboring the nitrogen atom.[9] That could indicate that neutral and protonated HMI are present in the MCM-22 precursor sample. Finally, infrared spectra of the precursor showed NH_2^+ bending bands, indicating that the template consists mainly of $HMIH^+$ cations.[10]

According to Lawton et al.,[9] ion exchange sites are mainly located in the sinusoidal channels in an amount of 5.5 ions/unit cell for a SiO_2/Al_2O_3 molar ratio of 21. Two types of these sites exist within the sinusoidal channels and may accommodate $HMIH^+$ moieties; depending on their orientation, up to 5 $HMI(H^+)$/unit cell can yield the full occupancy of both sites.

Concerning ion site exchange, the only Rietveld based analysis of a MCM-22 zeolite is reported in our paper on the Cu cation location.[13] A Rietveld based analysis of a transformation from layered to zeolite materials was reported recently on the preparation of B-RUB-41 from B-RUB-39.[14] Other studies by ESR[15] and also ESEM[16] on Ni-containing MCM-22 can be found. Both

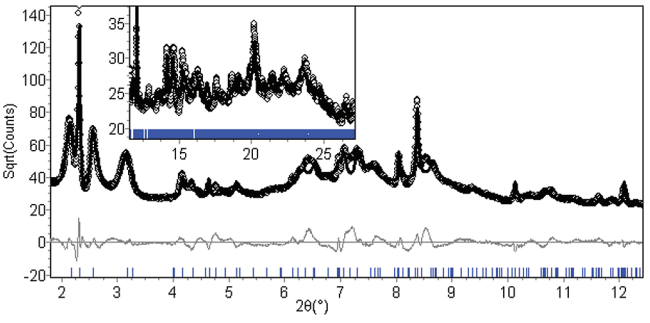

Figure 4. Observed (open circles), calculated (solid line), and difference plots of the final Rietveld refinement on the 373 K sample.

studies agree on the fact that the majority (about 70%) of the total cationic sites available for the exchange of small ions are inside the sinusoidal channels, the rest of them being placed in the supercages. For larger cations such as $HMIH^+$, steric hindrance may change this ratio.

Temperature programmed base desorption (TPBD) analysis[9] indicated that the low temperature HMI decomposition (473−623 K) occurs for molecules in the interlayer region, while

dx.doi.org/10.1021/cm201464j |*Chem. Mater.* 2011, 23, 4900–4909

high temperature peaks (623−773 K) correspond to the decomposition of HMI molecules in the intralayer-10 MR channels. TGA data[6,17] allowed estimating HMI content at the various temperatures, and the values have been used as a comparison for the HMI content in the various Rietveld refinements.

The picture emerging from the literature shows a number of open questions about (i) the location of the organic moiety sites in the channel system and in the intra- or interlayer system and (ii) the situation at the interface between layers during the thermal induced removal of HMI molecules. A careful study of the transformations from the layered solid to the tridimensional one and the role played by the guests on that process is of paramount importance, not only to understand the transformation itself but mainly to control and design improved procedures for the organic elimination and activation of the materials, with the final aim of obtaining better catalysts and membranes. Only a Rietveld based analysis can shed light on the distribution of species into the channels of complex materials.[18−20]

X-ray powder diffraction (XRPD) was employed to localize the hexamethyleneimine (HMI) organic molecules inside the zeolite channels during the MCM-22 calcination process. MO theoretical calculations, applying both periodic and cluster approaches, were performed to shed light on the real symmetry of the calcined MCM-22 phase and on the features of the interlayer interactions in the MCM-22 precursor.

2. EXPERIMENTAL SECTION

2.1. Sample Synthesis. Zeolite MCM-22 was prepared by hydrothermal treatment of a gel with the following composition: $4.44Na_2O{:}30SiO_2{:}Al_2O_3{:}17.76HMI{:}889H_2O$ at 423 K and 60 rpm for 7 days.[21] In the as-prepared MCM-22 precursor, the Si/Al ratio by elemental analysis was 27.3, resulting in 2.64 Al atoms per unit cell.[6] 10.4 HMI molecules per unit cell were found by TGA data, assuming that all weight losses above 373 K are due to HMI molecules. With these data, the resulting chemical formula per unit cell is $Si_{69.4}Al_{2.6}O_{144}{\cdot}(C_6NH_{13})_{10.4}$.[6,22] The MCM-22 precursor sample was inserted into a boron glass capillary (diameter 1 mm) connected to a vacuum line, heated at 373 K for 5 h to remove air moisture, and finally sealed to prevent contamination from air moisture. A milder 373 K heating (instead of the 423 K treatment used for the other three samples) was used to avoid the condensation of the layers and/or removal of structural HMI molecules, and this sample was named "373 K sample".

Three different samples have been obtained from the MCM-22 precursors by thermal treatment at 523, 623, and 823 K in O_2 atmosphere for 6 h. Then, each sample was introduced in a capillary and each capillary was connected separately to a vacuum line, outgassed for 5 h in vacuum at 423 K to remove adsorbed water molecules, and finally sealed to prevent contamination from air moisture, which might be mistaken for extra HMI in the Rietveld refinements. In fact, the as-prepared MCM-22 precursor without any treatment contains a noncontrollable amount of water and some disordered HMI molecules. This "as-made sample" shows an XRPD pattern similar to that of the 373 K sample, but with a larger background contribution and uncertainty about water content depending on air temperature and humidity during capillary preparation. Comparison between XRPD data from a sample of MCM-22 sealed in vacuum and exposed to air can be found in Figure 2 of ref 21.

2.2. Data Collection and Refinement. The four samples were analyzed by high resolution synchrotron radiation powder diffraction, at the SNBL (Swiss-Norwegian Beam Line) diffraction beamline.[23] The X-ray powder patterns were collected at 100 K using a wavelength of 0.50004 Å. Because of the layered morphology, a large anisotropic broadening effect was observed for all the samples, together with the instrumental peak asymmetry. Spherical harmonic functions,[24] available in the TOPAS[25,26] software, were employed to model such complex profile.

The *P6/mmm* structure of the calcined MCM-22 exposed to air, determined by Leonowicz et al.,[27] was used as the starting model for the sample heated at 823 K, and the Rietveld refinement of the structure was carried out using the TOPAS software.

The 823 K refined model was then used to start the analysis of the sample at 623 K, to locate the HMI molecules. In the first refinement steps, all parameters, except the background, were kept fixed. From this refinement it was possible to reveal the HMI molecules in a observed maximum entropy map, using the programs Rietan2000[28] and PRIMA.[29] To compute the maximum entropy map, the uniform prior density and the zero order single-pixel approximations were used.[30,31] To extract the observed intensities, the peak shapes were described in Rietan2000 with a modified split pseudo-Voigt function applicable to "relaxed" reflections.[28] The final location of the template was obtained by global optimization, using the TOPAS software.[25,26] The HMI molecules were treated as rigid bodies. Optimizations were performed on models with either two or three possible independent molecules of HMI. The final best solution was the one with three different positions for the HMI, not only yielding, as expected, better agreement factors but also allowing the filling of the channels without unwanted steric hindrance.

The analysis of the sample heated at 523 K followed a similar procedure to locate independently the HMI molecules. The only difference was that, in this case, the framework structure refined at 623 K was taken as starting point. The HMI molecules were located in positions close to those of the 623 K sample, indicating a rather good reproducibility of the Rietveld refinements.

For the precursor outgassed at 373 K, the analysis was made quite difficult by the poor crystallinity of the sample. However, it was possible to obtain a quite accurate crystallographic unit cell. To refine this diffraction pattern, the starting model was taken from the refined model at 523 K with three HMI molecules; only the rigid body positions of the HMI molecules, the profile parameters, the background, the cell parameters, the scale factor, and the occupancy parameters of Si and O atoms were refined.

In the final refinement, for the samples at 823, 623, and 523 K, a soft distance restraint of 1.61 ± 0.01 Å was imposed on the T−O bonds. The atomic displacement parameters (ADPs) were refined as an overall parameter, using a common ADP for Si, O, C, and N atoms, with the constraint that the ADP of Si is half that of the O and a quarter of that of the C and N atoms in HMI. The H atoms of the HMI molecule were not included in the model.

Graphical manipulation and output have been performed using Material Studio,[32] VESTA,[33] and Moldraw[34] software.

2.3. Theoretical Calculations. The periodic calculations were carried out employing the *ab initio* CRYSTAL code.[35] The fixed-cell unconstrained optimization of the atomic coordinates of the ordered model structures was performed by fixing the cell parameters to the values obtained from the X-ray diffraction experiments and employing a 3-21G basis sets, at the Hartree−Fock (HF)[36] level of theory.

Molecular orbital (MO) calculations with the cluster approach were performed with the Jaguar software[37] employing the DFT method based on Becke's exchange and the Lee, Yang, and Parr correlation functional[38] (named BLYP from now on). The Si and Al atoms were described using the LAV3P relativistic effective core potential (ECP).[39,40] The other atoms were described using the 6-31G basis sets.[36]

3. RESULTS AND DISCUSSION

Figure 3 shows the XRPD patterns of three samples treated at increasing temperatures and of the outgassed MCM-22 precursor (373 K sample).

The 373 K sample presents a typical powder pattern of a layered structure, while, after a mild treatment at 523 K, the MWW zeolitic framework is formed without the elimination of structurally ordered HMI molecules, as suggested by thermogravimetric analysis (TGA).[6,22] The thermal structural modifications undergone by the sample upon evolving from the layered precursor induce some important changes in the XRD pattern: the peaks in the sample treated at 523 K are much sharper than those in the 373 K pattern, which shows broad (00*l*) reflections, typical of the layered structure. With the increasing temperature, these peaks become sharper, with the (002) being superimposed to the (010) peak, as reported by Lawton et al.[8,9] The evolution of the diffraction patterns as a function of temperature shows significant modifications of the relative intensity of the peaks in the 1.5−5° 2θ range (d range 19.100−5.731 Å). This behavior is related to the progressive elimination of the organic molecules from the interlayer channels.

3.1. Precursor at 373 K. The result of the final refinement of the XRPD pattern is shown in Figure 4. The value of the *c*-axis is 26.282(9) Å, and it decreases by 1.15 Å (see also Table 3 for the final figures of merit of the refinements) when converting to the zeolite framework at 523 K (see section 3.2). The difference between the interlayer distance in the cases of covalent and noncovalent bonding between sheets was estimated by quantum-chemical molecular orbital calculations, employing two simplified cluster models, depicted in Figure 5, in which 100% and 0% of covalent bonds are present. Other cluster models can be conceived, including charged Si−O$^-$···HO−Si or [SiOAl]$^-$···HO−Si interactions and possibly inserting HMI molecules or cations. Because of the high deprotonation energy of the SiOH groups and the low Al content, the number of Si−O$^-$···HO−Si or [SiOAl]$^-$···HO−Si interactions must be rather limited in the crystalline material,[6] and any realistic model would not change dramatically the interlayer distance with respect to the adopted layered model. For these reasons, only the two extreme models in Figure 5 were considered. These two models are the simplest possible ones and are not meant to be fully realistic, but they are just meant to be a way to convey a better understanding of the situation at the interface between adjacent layers and to illustrate that, in the 373 K sample, neither the fully condensed nor the fully layered arrangements are present. Indeed, the interlayer distance observed in the 373 K sample is not consistent with either a condensed or a layered model, and an intermediate situation can be envisaged. In fact, the average Si−Si distances of the Si atoms pointing toward the interlayer space are directly related to the interlayer distance, because the inner structure of the lamellae is rigid; the cluster MO calculations indicate that this distance moves from 3.256 in the case of all covalent bonds between layers to 5.92 Å in the case of only H-bond interactions between layers. Therefore, if no Si−O bonds were present in the 373 K sample, the expected contraction for the 523 K sample would be about 2.66(5) Å. A similar use of bond and interlayer distance changes has been exploited by Grünewald-Lüke et al. to explain a transformation from a layered material to a 3D zeolite.[14] The smaller interlayer contraction observed during the zeolite formation (1.15 Å), together with the reduced concentration of silanols shown by IR data,[6] indicates that, in the precursor, the actual situation is intermediate between 0 and 100% of broken bonds, as shown in the two simplified models depicted in Figure 5, with a significant fraction of Si−O bonds already formed between the layers. The remaining interlayer bonds are represented by hydrogen bonds, surely charge-assisted by the HMI$^+$ cations, observed in the IR spectra.[41] The exact percentage of broken Si−O bonds cannot be estimated precisely because of the disorder of the sample. The real situation can be envisaged to be similar to that in the scheme represented in Figure 5, bottom, where the surface of the layers are deformed because of the Si−O−Si flexibility, and the layers are sometimes bonded and sometimes interacting only by hydrogen bonds, with a nonperiodic distribution of bonds, as suggested by the low crystallinity of the 373 K sample, shown by the broadening of the XRPD peaks.

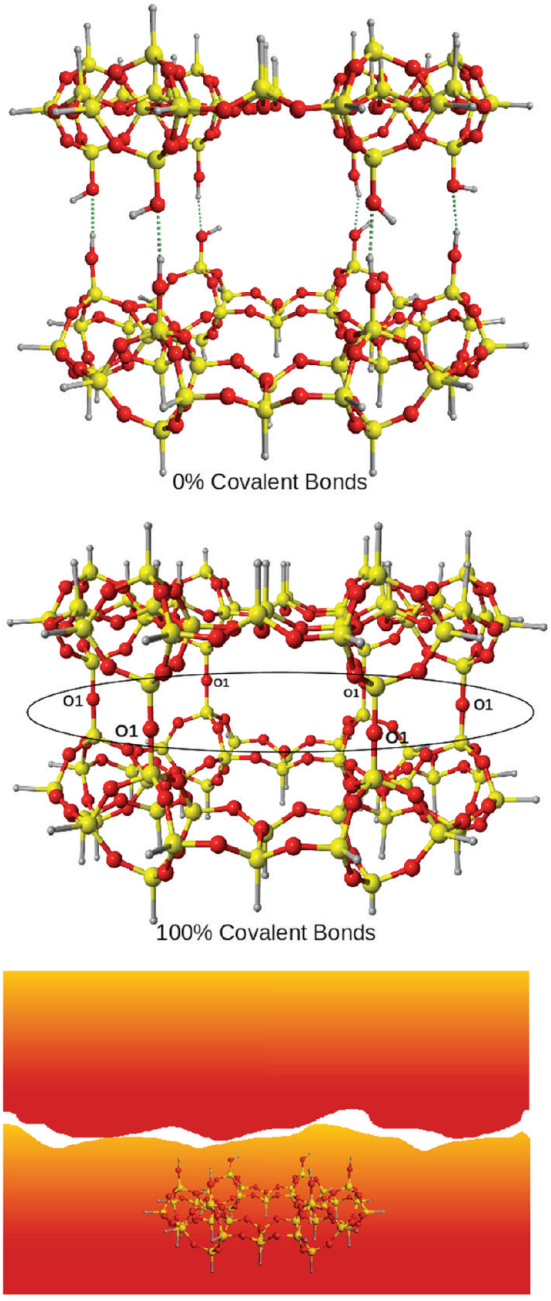

Figure 5. Condensed (top) and layered (middle) cluster models employed to investigate by MO calculations the interaction between the layers in the 373 K sample, together with a scheme of the disordered precursor.

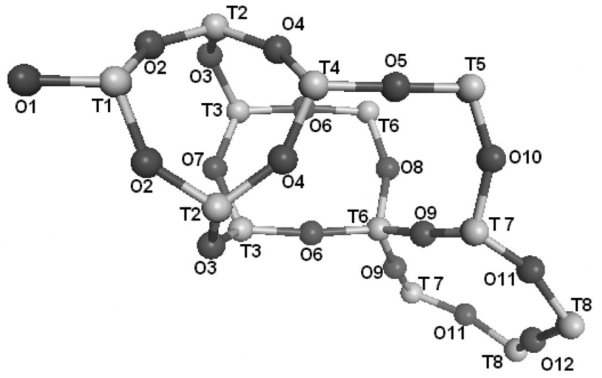

Figure 6. 3D arrangement of the relevant framework atoms.

Table 1. Final Occupancy Values of the T and O Sites[a]

atom	occupancy	atom	occupancy	atom	occupancy
T1	1.0(1)	O1	0.3 (2)	O9	1.00(4)
T2	1.00(5)	O2	0.71 (7)	O10	1.00(6)
T3	1.00(6)	O3	1.00(5)	O11	0.79(6)
T4	1.00(9)	O4	1.00(7)	O12	1.00(5)
T5	0.78(6)	O5	0.4(1)	O13	1.0(1)
T6	1.00(6)	O6	0.95(7)		
T7	0.97(4)	O7	0.84(7)		
T8	0.82(3)	O8	1.00(8)		

[a] Because of the poor quality of the diffraction pattern, the actual values obtained from the refinement may be higher than 1.00 (cf. Supporting Information), and they were set to 1.00.

Therefore, the best model for the 373 K sample is characterized by partially bonded layers with a high degree of heterogeneity of the interactions (covalent bonds, hydrogen bonds, and possibly ionic interactions between nonprotonated silanols and charged HMI^+ cations), as depicted in the scheme of Figure 5, bottom. It must be noted that the 373 K sample cannot be considered as the original "MCM-22 precursor" because of the pretreatment (5 h in vacuum at 373 K) that was necessary to have a set of comparable samples, all free of adsorbed water and of weakly physically bonded HMI molecules. This treatment might have reduced the defectivity in the 373 K sample with respect to the precursor at RT by removing some of the less stable pending silanols and inducing a partial condensation, but the change must be rather small because a significant amount of broken Si−O−Si bonds is still present, as indicated by the observed interlayer distance, which is significantly larger than that of a totally condensed situation, as discussed above. A fraction of silanols should be deprotonated to obtain charge neutrality, because the amount of deprotonated HMI (about 50% according to ref 12 and, thus, about 5 HMI/unit cell in the precursor and 4 and 3 HMI/unit cell in the 523 and 623 K samples, respectively) is larger than that of aluminum (2.63 atoms per unit cell, as detailed in the Experimental section).

As outlined in the Experimental section, starting from the model refined at 523 K with three different positions for the HMI molecules, the positions of the framework atoms (Figure 6) were kept fixed and only their occupancy was refined. The list of the occupancy values reported in Table 1 shows a very low value of 0.3(2) for atom O1 pointing toward the crossing window. This implies a very low electron density in this region and indicates a break of the interlayer bonds. Also, O2 and O5 occupancy, connecting

Table 2. Evolution in the Different Samples of the Occupancy of the O Atoms, Relevant for the Condensation Reaction

atom	occupancy 373 K	occupancy 523 K	occupancy 623 K	occupancy 823 K
O1	0.3(2)	1.00(4)	1.00(4)	1.00(4)
O5	0.4(1)	0.76(1)	0.72(3)	1.00(3)
O2	0.71(4)	0.95(1)	0.94(3)	1.00(1)

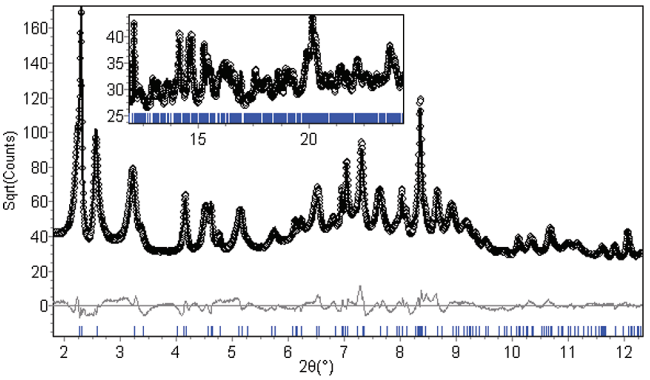

Figure 7. Observed (open circles), calculated (solid line), and difference plots of the final Rietveld refinement of the 523 K sample.

the different cages in a direction perpendicular to the layers, have rather low values.

Similar refinements were performed on all samples, and the values for the occupancy of O1, O5, and O2 are shown in Table 2. These data indicate that, at 523 K, the oxygen atoms bridging the layers (O1 in Figure 5) already reach an occupancy of 1 after this mild treatment, and the 3D zeolite is formed well before the elimination of all structurally ordered HMI molecules.

The HMI molecules are located in the sinusoidal and the straight channels, in positions similar to those of the sample at 523 K, but in the precursor, it is not possible to distinguish between the two different positions in the straight channel: the one in the 12-MR inner part of the supercage and the one in the center of the 10-MR crossing window. Refinements and simulated annealing were performed, as explained in details in section 3.3, but with no success, because the figures of merit remain very similar in both cases, thus indicating a lower degree of order with respect to the 523 K sample.

3.2. Sample at 523 K. The result of the final refinement of the XRPD pattern is shown in Figure 7 (cf. Table 3 for the final figures of merit). The lattice parameters are $a = 14.2607(5)$ Å and $c = 25.136(2)$ Å. The decrease by 1.15 Å of the c-axis indicates the formation of the zeolitic structure.

Two refinements were performed with two and three HMI molecules, but the latter solution turned out to be the best, as detailed in the Experimental section, and we will concentrate only on the second. The Monte Carlo procedure converged to the following described positions for the organic molecules.

The first, named molecule 1, was located in the sinusoidal channel (Figures 8 and 11). The center of mass of the molecules is located in the Wyckoff positions g at $0, {}^1/_2, {}^1/_2$ with multiplicity 3 and site symmetry mmm of the space group $P6/mmm$. Eight molecules will be generated around each of the 3 centers of mass to account for the multiplicity 24 of the general positions. The global occupancy of each molecule turned out to be 0.171(2),

dx.doi.org/10.1021/cm201464j |Chem. Mater. 2011, 23, 4900–4909

corresponding to 4.10(5) molecules in the unit cell. The analysis of the disorder and of the possible steric hindrance shows that 4 molecules/unit cell can be located without too short intermolecular contacts.

The second, named molecule 2, was located in the straight channel in the 12-MR inner part of the supercage (Figures 9 and 11). The center of mass of the molecules is located in the Wyckoff positions *e* at 0,0,*z* with multiplicity 2 and site symmetry 6*mm*. Twelve molecules will then be generated around each of the 2 centers of mass. The global occupancy of each molecule turned out to be 0.094(1), corresponding to 2.25(2) molecules in the unit cell. Two HMI molecules can be located without too short intermolecular contacts. The slightly higher values 2.25(2) obtained from the refinement can be explained by the error due to the correlation between occupancy and thermal factors and to the possible presence of some residual water molecules, as suggested by IR[10] and TGA data.[6]

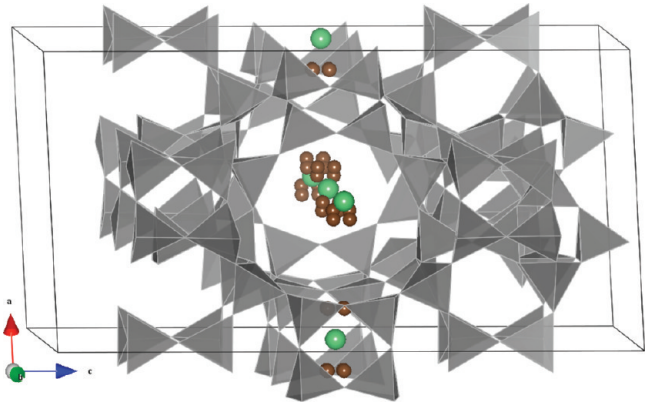

Figure 8. Brown: centers of mass of the HMI molecule 1, located in the sinusoidal channel. Green: the overall center of mass located in the Wyckoff positions *g* at 0,$^1/_2$,$^1/_2$ with multiplicity 3 and site symmetry *mmm*.

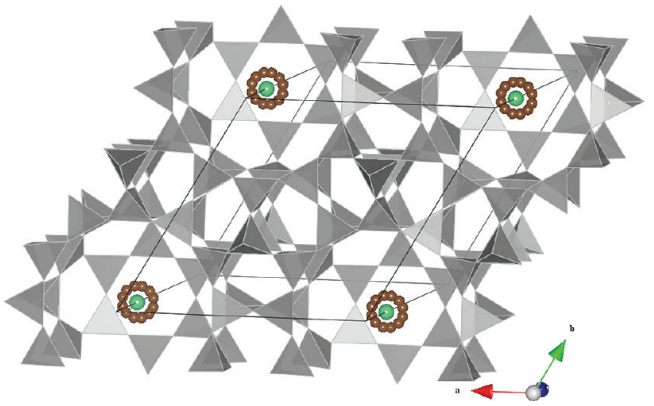

Figure 9. Brown: centers of mass of the HMI molecule 2, located in the straight channel in the 12-MR inner part of the supercage. Green: the overall center of mass located in the Wyckoff positions *e* at 0,0,*z* with multiplicity 2 and site symmetry 6*mm*.

The third, named molecule 3, was located in the center of the 10-MR crossing window, that is, in the center of the supercage (Figures 10 and 11). The center of mass of the molecules is located in the Wyckoff positions *a* at 0,0,0 with multiplicity 1 and site symmetry 6/*mmm*. Twenty-four molecules will then be generated around each center of mass. The global occupancy of each molecule turned out to be 0.074(1), corresponding to 1.77(2) molecules in the unit cell without too short intermolecular contacts. As shown in Figure 10, the centers of mass of the single molecules (brown dots) are arranged on two parallel layers separated by an *m* symmetry plane.

There is a total of 8.12(9) HMI molecules in the unit cell. The coordinates of the three HMI molecules are reported in Table A in the Supporting Information. These results are in agreement with the computational work of Zhou Dan-Hong.[42] TGA data[6] of the as-made MCM-22 precursor, without any pretreatment, suggest the presence of 10.4 HMI molecules per unit cell, assuming that the weight loss around 373 K is due to water and all weight losses above 373 K are due to HMI. This value (10.4) is similar to that obtained by other authors[10,11] and is larger than the expected one.[42] The difference between the value from TGA (10.4) and the one obtained by XRPD (8.12) is due to the treatment at 523 K that induces the elimination of weakly bound HMI, present at the surface, in defect sites, and in the layer region where Si−O−Si bonds are broken[43] and to the pretreatment (5 h at 373 K in vacuum employed to obtain identical standardized samples useful for a direct comparison), hindering the occupation of the left space by water coming from air moisture. The remaining 8.12 HMI molecules are thus more strongly bonded. Moreover, it must be pointed out that XRPD can detect only HMI molecules showing sufficient long-range order, and therefore, some less ordered molecules could be neglected, with an underestimation of the HMI content. Concerning

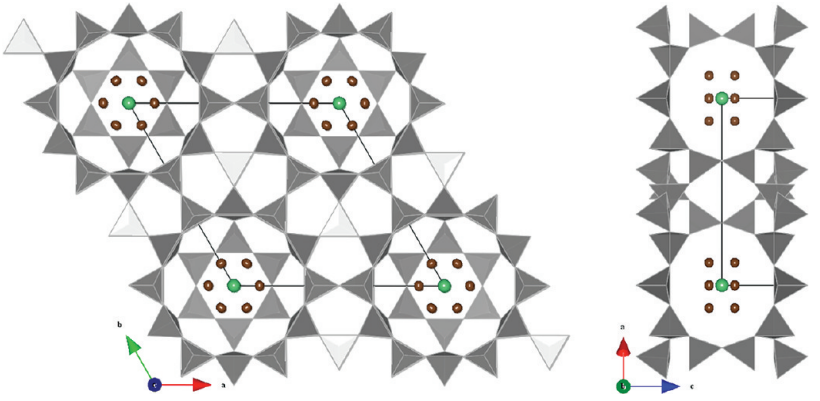

Figure 10. Brown: centers of mass of the HMI molecule 3, located in the center of the 10-MR crossing window. Green: the overall center of mass located in the Wyckoff positions *a* at 0,0,0 with multiplicity 1 and site symmetry 6/*mmm*.

dx.doi.org/10.1021/cm201464j |*Chem. Mater.* 2011, 23, 4900–4909

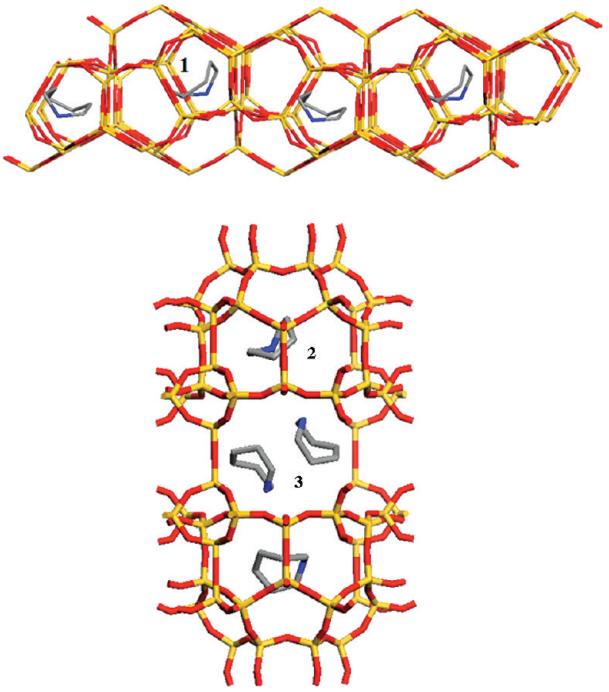

Figure 11. Position of HMI molecules in the sinusoidal channel (top, HMI molecule 1, also referred as "sinusoidal channel HMI" in the text) and in the supercage (bottom, molecules 2 and 3, referred as "12-MR inner part" and "center 10-MR", respectively).

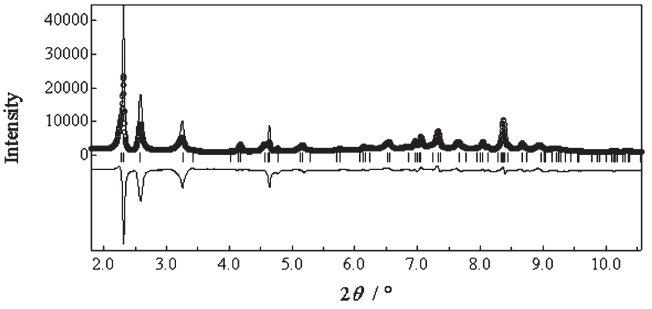

Figure 12. Observed (dotted line), calculated (solid line), and difference plots of the Rietveld refinement for the sample at 623 K; HMI is not yet present in the model.

the state of these molecules, according to the literature,[11,12] a relevant number of HMI molecules is protonated.

3.3. Sample at 623 K. As explained in the Experimental section, the P6/*mmm* structure of the calcined MCM-22 exposed to air, determined by Leonowicz et al.,[27] was used as starting model. The first refinement (Figure 12), using the program RIETAN-2000, converged to R_{wp} = 27.1, R_p = 14.7, and χ^2= 9.9. As expected, the fit is bad in the low theta region, as a result of the presence of the HMI molecules, not included in the model.

In the observed maximum entropy maps (Figures 13 and 14), computed using the program PRIMA,[29] it was possible to observe a residual density in the channels.

The atoms of the HMI molecule could not be localized manually in the maximum entropy map because of their disorder. Only the position of the centers of mass could be deduced. The molecules were finally localized by direct space optimization, carried out with the TOPAS software. In total, for each molecule

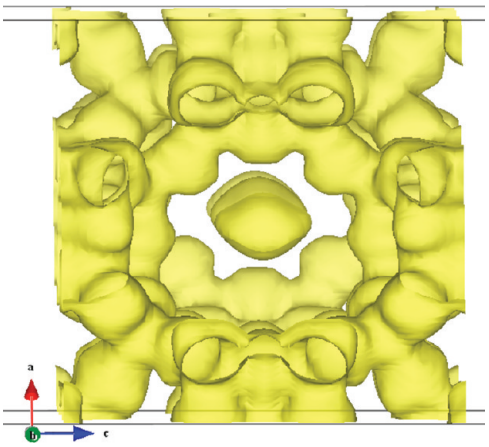

Figure 13. Observed density (molecule 1) in the sinusoidal channel around the Wyckoff positions *g* at $0,{}^1/_2,{}^1/_2$ with site symmetry *mmm*.

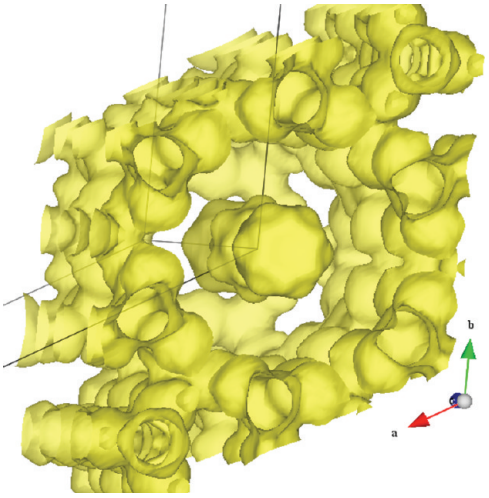

Figure 14. Observed density in the straight channel along the 6-fold axis: the density closer to the viewer is the one in the 12-MR inner part of the supercage (molecule 2) around the Wyckoff positions *e* at 0,0,*z* and site symmetry 6 *mm*, and the inner density is the one located at the center of the 10-MR crossing window (molecule 3) around the Wyckoff positions *a* at 0,0,0 and site symmetry 6/*mmm*.

3 translation, three rotation parameters and one global occupancy parameter were refined. No antibump parameter was used, and the molecules were free to move in the whole cell. The ADPs of the framework atoms were kept fixed at the same values obtained for the calcined sample at 823 K, as the data were collected at the same temperature. The ADPs of the HMI atoms were constrained, as described in the Experimental section, to a value of 3.3(2) Å^2. The results of the final refinement of the XRPD pattern is shown in Figure 15 (cf. Table 3 for the final figures of merit). This indicates a good agreement between the refined model and the experimental data.

As for the case of the 523 K sample, three independent HMI molecules were localized in the zeolite in the positions observed in the maximum entropy maps (Figures 13 and 14).

The first molecule (as in Figure 8, see also Figure 11 (top) and Figure A in the Supporting Information) was located in the sinusoidal channel, with a global occupancy of 0.146(1), [3.50(2) molecules/cell]; the second (as in Figure 9, see also Figure 11 (bottom)

dx.doi.org/10.1021/cm201464j |*Chem. Mater.* 2011, 23, 4900–4909

Table 3. Refined Unit-Cell Parameters and Final Figures of Merit for the Different Refinements of the Four Structures

sample T (K)	a (Å)	c (Å)	R_{wp} (%)	R_p (%)	χ^2
373	14.244(1)	26.282(9)	9.8	7.4	4.6
523	14.2607(4)	25.136(3)	6.2	4.8	3.5
623	14.2621(9)	25.072(2)	4.9	3.9	2.6
823	14.2533(5)	25.029(5)	6.2	4.6	3.2

and Figure B in the Supporting Information) was located in the straight channel in the 12-MR inner part of the supercage, with a global occupancy of 0.082(1) [1.96(2) molecules/cell]; and the third (as in Figure 10, see also Figure 11 (bottom) and Figure B in Supporting Information) was located in the center of the 10-MR crossing window, with a global occupancy of 0.054(1) [1.30(2) molecule/cell]. In total, there are then 6.76(6) molecules/unit cell. As expected, the number of HMI molecules is reduced with a decrease of the individual occupancies of the three different positions. Assuming that the more tightly bonded HMI molecules are protonated[11] and that about half of them are charged in the MCM-22 precursor, the 623 K sample, where 40% of the formerly present HMI molecules are eliminated (4 out of the starting 10.42 from TGA data), should mainly contain protonated HMI.

3.4. Calcined Sample at 823 K. The organic phase is completely removed and no extra-framework atoms have been found, as indicated by the almost flat difference curve in Figure 16, showing the result of the final refinement (cf. Table 3 for the final figures of merit). This is confirmed also by the observed maximum entropy map, which does not show any density in the channels. The ADPs converged to the value 0.83(5) Å^2 for the Si atoms and 1.6(1) Å^2 for the O atoms.

The deviations from the expected value of 1.61 Å of the T−O bond lengths are reported in Table B of the Supporting Information and arise because, in the space group *P6/mmm*, all the atoms except O9 and O3 lie in special positions. As proposed by Leonowicz et al.,[27] the actual space group should be *Cmmm*, but the poor crystallinity and the pseudo symmetry of the siliceous framework make the refinement in the lower symmetry totally unstable.

MO periodic calculations were performed to shed light on the real symmetry of the calcined MCM-22 phase and indicated that the *Cmmm* symmetry allows a more relaxed structure with respect to the *P6/mmm* one, mandatory for a stable Rietveld refinement. No aluminum atom was inserted in the calculations; indeed, with 2.63 Al atoms per unit cell, a correct periodic model with Al atoms distributed in all possible T sites would require a supercell containing more than four MCM-22 unit cells, the result of which would be too large to be treated at MO level in a acceptable computation time. Indeed, its distribution is probably random with some weakly preferred T site, as observed in previous experimental[19] and computational[44] studies. Actually, the only significant distortion was observed for the Si−O1−Si angle (Figure 5) that moved from 180° (value imposed by *P6/mmm*) to 160.8° after the computational optimization in *Cmmm*. The overall shape and size of the supercage was retained, and also, the sinusoidal channel was not changed, thus confirming that the *P6/mmm* space group, despite the unreasonable value of 180° imposed to the Si−O1−Si angle, is still a good approximation of the real structure of MCM-22. Attempts at Rietveld refinement of the MCM-22 structure using the *Cmmm* symmetry diverged (as also tested with a different refinement strategy

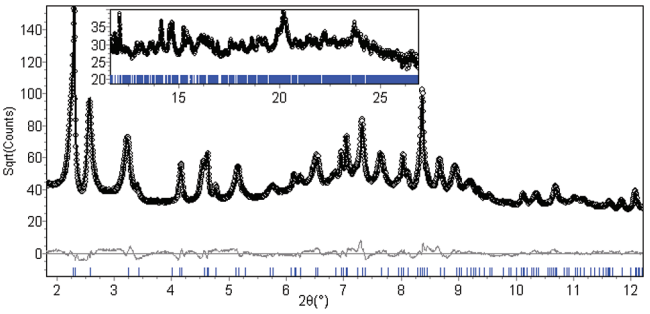

Figure 15. Observed (dotted line), calculated (solid line), and difference plots of the final Rietveld refinement of sample 623 K.

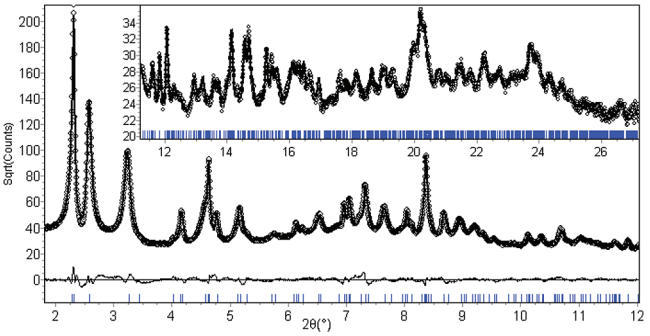

Figure 16. Observed (dotted line), calculated (solid line), and difference plots of the final Rietveld refinement of sample 823 K.

approach, using the GSAS software in our previous work on copper MCM-22[13]), because of the correlations induced by the overwhelming *P6/mmm* symmetry, constraints, and/or damping should be used for all but two atoms (Si1 and O1), without significant differences from the *P6/mmm* refinement. In fact, the theoretical calculations indicated that the structure of the layer remained very similar to that of the experimental *P6/mmm* structure, revealing a rigid behavior of the MCM-22 lamellae, while only the interlayer connections through oxygen O1 were affected. Therefore, the Si−O1−Si angle of 180°, observed in the experimental crystal structure, can be explained with a dynamical disorder of the oxygen atom; assuming an angle of 160°, as indicated by the theoretical calculations, the oxygen atom is rotated by the 6-fold symmetry around the 6-fold axis, and the result is a linear Si−O1−Si moiety along this axis. The expected shortening of about 0.1 Å of the Si−O1 bond length because of the 180° Si−O1−Si angle is not observed, and it can be argued that the real Si−O1−Si angle is closer to 180° than the calculated value (160.8°). A rigid body adopting higher symmetry and imposing this symmetry to the whole structure is a phenomenon often observed in zeolites.[19] Such flexibility of Si−O−Si and Me−O−Si bonds (where Me stays for Ga, B, Ti, for instance) was already observed for Ga-zeolites by powder X-ray diffraction,[45] in which the insertion of small amounts of Ga (with an atomic radius larger than Si) induces a decrease of lattice parameters, because of the easy change of the Ga−O−Si angles. This behavior is quite common in zeolites[46,47] and has been observed also by single crystal data.[48]

3.5. Comparison of Structural Parameters in the Different Samples. In Table B of the Supporting Information, the final bond lengths for the different T−O sites are reported, and in Table 3, the

Table 4. Change of Occupancy of HMI Molecules Per Cell and Percentage of Elimination (% Elimination) for Each Site in Going from 523 to 623 K

HMI site	523 K	623 K	% elimination
1	4.10(5)	3.50(2)	15(1)
2	2.25(2)	1.96(2)	13(1)
3	1.77(2)	1.30(2)	27(1)
total	8.12(9)	6.76(6)	17(1)

refined unit-cell parameters and the final figures of merit for the different refinements with three HMI molecules are reported. In general, the heating of zeolites induces a contraction of the lattice parameters due to organic elimination.[49] This trend is, in general, observed also in the MCM-22 case, but with a rather strong anisotropy, the *a*-axis is almost unchanged, while *c* changes by more than 1 Å. This is in agreement with the layered nature of MCM-22 and depends on the fact that heating induces the above-described (section 3.1) condensation of the Si−O dangling bonds lying along the *c*-axis.

The occupancies of the HMI molecules were refined independently, and this allowed the envisaging of a different elimination degree for molecules located in different sites. It was then possible to calculate the percentage of elimination (Table 4 last column), that is, the relative amount of each HMI in the three positions (1, 2, and 3 in Figure 11) eliminated from 523 to 623 K. This information is interesting because it demonstrates that the HMI molecules in different sites behave differently; that is, molecule 3 is eliminated in a larger amount (27%) than the other two (13 and 15%), indicating that molecule 3, in the center of the 10 member ring, is preferentially eliminated at 623 K. This behavior can be explained by the longer distances from the siliceous framework observed for this molecule, thus resulting in weaker interactions with respect to molecules 1 and 2. It might be inferred that the site of molecule 3, far away from the negatively charged sites of the framework, accommodates preferentially neutral HMI molecules, which are easily eliminated during the thermal treatment.

4. CONCLUSIONS

By studying four different steps along the heating process from the precursor to the final calcined sample, it has been possible to describe the evolution of the crystal structure, going from the layered MCM-22 precursor to a 3D MCM-22 zeolitic structure.

Starting from the maximum entropy maps, real space optimization, and refinement of XRPD data allowed the location of the HMI molecules into the zeolitic channels. There are three different positions occupied. One is located in the sinusoidal channel, and the other two are in the straight channel, in the 12-MR inner part of the supercage and in the center of the 10-MR crossing window, respectively. At 523 K, there are 8 HMI molecules/unit cell, four located in the sinusoidal channel, two in the straight channel in the 12-MR inner part of the supercage and two in the center of the 10-MR crossing window. The full elimination of organic molecules was obtained after the treatment at 823 K, as revealed by the absence of extra framework peaks in the calcined sample. Concerning the siliceous 3D framework, it is worth noting that it is already formed at 523 K, with the formation of Si−O−Si covalent bonds between two adjacent layers, with the elimination of less ordered and weakly bonded HMI molecules (probably located at defect sites, at the surface and in the interlayer region), with 8.16 HMI molecules per unit cell still present in the channels. While HMI plays a major role in the condensation from the MCM-22 precursor to the 523 K sample, the elimination of the remaining 8.16 HMI molecules above 523 K proceeds without interfering with the framework stability. Besides, in the MCM-22 precursor (sample treated at 373 K), the presence of dangling Si−O bonds, to explain the larger interlayer distance and the low occupancy of oxygen atoms bridging two adjacent layers, was proved by MO calculation with cluster approach. The actual MCM-22 symmetry was also explored by periodic MO calculations. In fact, the higher symmetry *P6/mmm* space group is mandatory for a stable Rietveld refinement, because of the dominant pseudosymmetry of the siliceous framework, but it yields unrealistic Si−O−Si bonds connecting the layers with angles of 180°. The computational optimization of the structure in the *Cmmm* space group gave a chemically reliable result, with Si−O−Si bonds assuming an angle of 160.8°. A paper dedicated to the computational study of MCM-22 by the first principle periodic approach, using DFT functional with specific corrections apt to treat dispersion interaction, is in preparation. Finally, it is worth noting that the combination of different crystallographic and computational methods is successful also in this kind of rather complicated samples and can be adopted for other layered system.

■ ASSOCIATED CONTENT

Supporting Information. Crystallographic data (distances and angles tables and crystal structure files in cif format), detailed pictures of HMI molecules into MCM-22 channels and of all XRPD Rietveld refinements. This information is available free of charge via the Internet at http://pubs.acs.org/.

■ AUTHOR INFORMATION

Corresponding Author

*Fax: + 39 0131 360250. Tel.:+ 39 0131 360226. E-mail: marco.milanesio@mfn.unipmn.it.

■ ACKNOWLEDGMENT

Our first thanks are due to L. Marchese of our department and to H. O. Pastore, E. C. O. Munsignatti and S. R. Dutra of the Instituto de Química, Universidade Estadual de Campinas, Brazil, for suggesting this work and supplying the samples, together with useful advice. We would like to thank A. Coelho (Coelho Software Brisbane, Australia) for his advice and especially for the use of the spherical harmonic functions in the TOPAS program and F. Izumi (National Institute for Materials Science, Tsukuba) for his advice and help in using the modified split pseudo-Voigt function for relaxed reflections in RIETAN2000. W. van Beek (SNBL, Grenoble, France) is acknowledged for technical support during the X-ray powder diffraction measurements and ESRF for beam time (proposal CH-1423). We would like to thank Dr. Yi Hong (daughter-in-law of D. V.) for translating ref 39. MIUR (PRIN-2007 project: "Sviluppo di nanocompositi ibridi "host-guest" per il rilascio modificato di farmaci mediante approcci innovativi di caratterizzazione sperimentale a livello molecolare") and Fondazione CRC (Grant No. 2008-1581) are gratefully acknowledged for funding. L. P. acknowledges Nova Res S.r.l. (http://www.novares.org) for cofunding his bursary.

■ REFERENCES

(1) Meier, W. M.; Olson, D. H.; Baerlocher, C. H. *Atlas of Zeolite Structure Types*; Elsevier: London, 1996.

(2) Puppe, L.; Weisser, J. U.S. Patent No. 4.439.409, 1984.
(3) Ban, S.; Laak, A.; de Jongh, P. E.; van der Eerden, P. J. M.; Vlugt, J. H. *J. Phys. Chem. C* **2007**, *111* (46), 17241–17248.
(4) Wang, S.; Li, H.; Xu, L. *J. Colloid Interface Sci.* **2006**, *295*, 71–8.
(5) Pirngruber, G.; Seshan, K.; Lercher, J. A. *J. Catal.* **2000**, *190*, 396–405.
(6) Santos Marques, A. L.; Monteiro, J. L. F.; Pastore, H. O. *Microporous Mesoporous Mater.* **1999**, *32*, 131.
(7) Corma, A.; Fornes, V.; Pergher, S. B.; Maesen, Th. L. M.; Buglass, J. G. *Nature* **1998**, *396*, 353–356.
(8) Lawton, S. L.; Leonowicz, M. E.; Partridge, R. D.; Chu, P.; Rubin, M. K. *Microporous Mesoporous Mater.* **1998**, *23*, 1–2.
(9) Lawton, S. L.; Fung, A. S.; Kennedy, G. J.; Alemany, L. B.; Chang, C. D.; Hatzikos, G. H.; Lissy, D. N.; Rubin, M. K.; Timken, H.-K. C.; Steuernagel, S.; Woessner, D. E. *J. Phys. Chem.* **1996**, *100*, 3788–3798.
(10) Corma, A.; Corell, C.; Fornés, V.; Kolodziejski, W.; Pérez-Pariente, J. *Zeolites* **1995**, *15* (7), 576–582.
(11) Corma, A; Corell, C.; Pérez-Pariente, J. *Zeolites* **1995**, *15* (1), 2–8.
(12) Testa, F.; Crea, F.; Diodati, G. D.; Pasqua, L.; Aiello, R.; Terwagne, G.; Lentz, P.; Nagy, J. B. *Microporous Mesoporous Mater.* **1999**, *30*, 187–197.
(13) Milanesio, M.; Croce, G.; Viterbo, D.; Pastore, H. O.; dos Santos Mascarenhas, A. J.; de Oliveira Munsignatti, E. C.; Meda, L. *J. Phys. Chem. A* **2008**, *112* (36), 8403–8410.
(14) Grünewald-Lüke, A.; Gies a, H.; Müller, U.; Yilmaz, B.; Imai, H.; Tatsumi, T.; Xie, B.; Xiao, F. S.; Bao, X.; Zhang, W.; De Vos, D. *Microporous Mesoporous Mater.* **2012**, *147* (1), 102–109.
(15) Prakash, A. M.; Kevan, L. *J. Phys. Chem.* **1996**, *100* (50), 19587–19594.
(16) Wasowicz, T.; Prakash, A. M.; Kevan, L. *Microporous Mater.* **1997**, *12*, 107–116.
(17) Albuquerque, A.; Marchese, L.; Lisi, L.; Pastore, H. O. *J. Catal.* **2006**, *241*, 367–377.
(18) Agostini, G.; Lamberti, C.; Palin, L.; Milanesio, M.; Danilina, N.; Xu, B.; Janousch, M.; van Bokhoven, J. A. *J. Am. Chem. Soc.* **2010**, *132* (2), 667–678.
(19) Palin, L.; Lamberti, C.; Kvick, Å.; Testa, F.; Aiello, R.; Milanesio, M.; Viterbo, D. *J. Phys. Chem. B* **2003**, *107* (17), 4034–4042.
(20) Sánchez del Río, M.; Boccaleri, E.; Milanesio, M.; Croce, G.; Beek, W.; Tsiantos, C.; Chyssikos, G. D.; Gionis, V.; Kacandes, G. H.; Suárez, M.; García-Romero, E. *J. Mater. Sci.* **2009**, *44*, 5524–5536.
(21) Milanesio, M.; Croce, G.; Frache, A.; Mascarenhas, A. J. S.; Oliveira, E. C. *Stud. Surf. Sci. Catal.* **2005**, *155*, 415–426.
(22) Leite, R. C. N.; de Sousa, B. V.; Rodrigues, M. C. F. *4° PDPETRO*, Campinas, SP, 2007, 4.2.0191−1.
(23) Experiment carried out at the Swiss-Norwegian Beam Line (SNBL) the ESRF, Grenoble, France, (http://www.snbl.eu) proposal CH-1423.
(24) Coelho, A. *Technical Reference Manual*, TOPAS-Academic by Coelho Software, 2006.
(25) Coelho, A. *J. Appl. Crystallogr.* **2000**, *33* (3), 899–908.
(26) Coelho, A. *J. Appl. Crystallogr.* **2005**, *38* (3), 455–461.
(27) Leonowicz, M. F.; Lawton, J. A.; Lawton, S. L.; Rubin, M. K. *Science* **1994**, *264*, 1910–1913.
(28) Izumi, F.; Ikeda, F. *Mater. Sci. Forum* **2000**, *198*, 321–324.
(29) Izumi, F.; Dilanian, R. A. *Recent Research Developments in Physics*, Part II; Transworld Research Network: Trivandrum, India, 2002; Vol. 3, pp 699−726.
(30) Kumazawa, S.; Kubota, Y.; Takata, M.; Sakata, M.; Ishibashi, Y. *J. Appl. Crystallogr.* **1993**, *26* (3), 453–457.
(31) Kumazawa, S.; Takata, M.; Sakata, M. *Acta Crystallogr. A.* **1995**, *51* (1), 47–53.
(32) *Material Studio 4.0*; Accelrys Software Inc.: 2001−2006
(33) Momma, K.; Izumi, F. *J. Appl. Crystallogr.* **2008**, *41*, 653–658.
(34) Ugliengo, P.; Viterbo, D.; Chiari, G. *Z. Kristallogr.* **1993**, *207*, 9–23.
(35) Saunders, V. R.; Dovesi, R.; Roetti, C.; Causà, M.; Harrison, N. M.; Orlando, R.; Zicovich-Wilson, C. M. *CRYSTAL-98 User's Manual*. Università di Torino: Torino, Italy, 1999.
(36) Hehre, W. J.; Radom, L.; Schleyer, P. v. R.; Pople, J. A. *Ab Initio Molecular Orbital Theory*; Wiley: New York, 1986.
(37) *Jaguar Version 5.5*; Schrödinger Inc.: Portland, OR, 2003.
(38) Lee, C.; Yang, W.; Parr, R. G. *Phys. Rev. B* **1988**, *37*, 785–789.
(39) Hay, P. J.; Wadt, W. R. *J. Chem. Phys.* **1985**, *82*, 270–283.
(40) Wadt, W. R.; Hay, P. J. *J. Chem. Phys.* **1985**, *82*, 284–298.
(41) Ferretti, V.; Bertolasi, V.; Pretto, L. *New J. Chem.* **2004**, *28*, 646–651.
(42) Zhou, D.; Yang, M.; Wang, Y.; Yang, G.; Liu, X. C. *Chin. J. Chem.* **2004**, *20* (1), 41–47.
(43) Mochida, I.; Eguchi, S.; Hironaka, M.; Nagao, S.; Sakanishi, K.; Whitehurst, D. D. *Zeolites* **1997**, *18*, 142–151.
(44) Ricchiardi, G.; de Man, A.; Sauer, J. *Phys. Chem. Chem. Phys.* **2000**, *2*, 2195–2204.
(45) Fricke, R.; Kosslick, H.; Lischke, G.; Richter, M. *Chem. Rev.* **2000**, *100*, 2303–2405.
(46) Gibbs, G. V. *Am. Mineral.* **1982**, *67*, 421–450.
(47) Shluger, A. *J. Phys. Chem. Solids.* **1986**, *47*, 659–467.
(48) Zema, M.; Tarantino, S. C.; Montagna, G. *Chem. Mater.* **2008**, *20*, 5876–5887.
(49) Milanesio, M.; Artioli, G.; Gualtieri, A. F.; Palin, L.; Lamberti, C. *J. Am. Chem. Soc.* **2003**, *125* (47), 14549–14558.